Direct Simulations of Anharmonic Infrared Spectra Using Quantum Mechanical/Effective Fragment Potential Molecular Dynamics (QM/EFP-MD): Methanol in Water

ARTICLE *in* THE JOURNAL OF PHYSICAL CHEMISTRY A · AUGUST 2012

Impact Factor: 2.69 · DOI: 10.1021/jp306807v · Source: PubMed

4 AUTHORS, INCLUDING:

Manik Ghosh
University of Limerick
26 PUBLICATIONS **167** CITATIONS
SEE PROFILE

Cheol Ho Choi
Kyungpook National University
111 PUBLICATIONS **2,123** CITATIONS
SEE PROFILE

Minhaeng Cho
IBS, Korea University
217 PUBLICATIONS **7,470** CITATIONS
SEE PROFILE

THE JOURNAL OF PHYSICAL CHEMISTRY A

Article

pubs.acs.org/JPCA

Direct Simulations of Anharmonic Infrared Spectra Using Quantum Mechanical/Effective Fragment Potential Molecular Dynamics (QM/EFP-MD): Methanol in Water

Manik Kumer Ghosh,[†] Jooyong Lee,[‡] Cheol Ho Choi,*[,†] and Minhaeng Cho*[,‡,§]

[†]Department of Chemistry and Green-Nano Materials Research Center, College of Natural Sciences, Kyungpook National University, Taegu 702-701, South Korea

[‡]Department of Chemistry, Korea University, Seoul 136-713, Korea

[§]Multidimensional Spectroscopy Laboratory, Korea Basic Science Institute, Seoul 136-713, Korea

ABSTRACT: One of the most stringent tests for chemical accuracy of a hybrid quantum mechanical/molecular mechanical (QM/MM) molecular dynamics simulation method would be to directly compare the calculated vibrational spectra with the corresponding experimental results. Here, the applicability of hybrid QM/effective fragment potential (EFP) to the simulations of methanol infrared spectra is investigated in detail. It is demonstrated that the QM/EFP simulations in combination with time correlation function theory yield not only the fundamental transition bands but also the major overtone and combination bands of methanol dissolved in water in both mid- and near-IR regions. This clearly indicates that the QM/EFP-molecular dynamics can be a viable way of obtaining an anharmonic infrared spectrum that provides information on solvatochromic frequency shifts and fluctuations, solute−solvent interaction-induced dephasing, and anharmonic coupling effects on vibrational spectra of aqueous solutions. We anticipate that the computational protocol developed here can be effectively used to simulate both one- and two-dimensional vibrational spectra of biomolecules and chemically reactive systems in condensed phases.

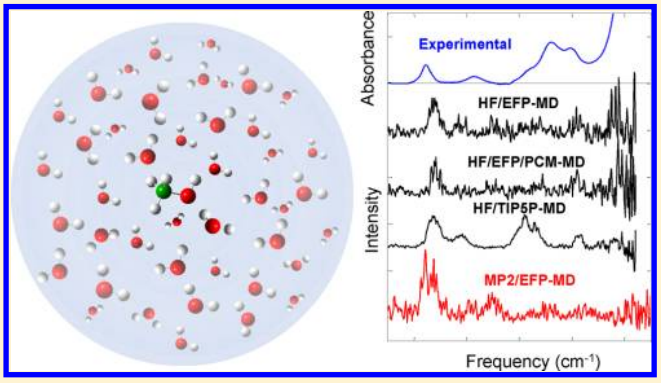

1. INTRODUCTION

It has been known from the classical molecular dynamics (MD)[1] that simulations for 100−200 ps/window are necessary to guarantee sufficient samplings of hydration dynamics. Although ab initio molecular dynamics (AIMD) simulation methods such as Car−Parrinello MD(CPMD)[2] or FMO-MD[3] have been recognized to be one the most direct and accurate computational tools for studying such dynamic processes in condensed phases, the AIMD simulation over such a long time period for fairly large composite systems is still far from practical. To overcome this difficulty, the quantum mechanical/molecular mechanical (QM/MM) method has been successfully used as an alternative method.[4] However, in the cases that water molecules play essential roles in determining physical and chemical dynamics and relevant time scales, the retention of a clear boundary between QM and MM water molecules during long-time simulations is often problematic since QM and MM water may naturally exchange with each other, which thereby eventually removes the QM/MM boundary.

As an alternative approach, the classical MM force field can be replaced with the quantum mechanically driven force field. Gao and co-workers developed an explicit polarization (X-Pol) model.[5,6] In this case, the entire system is divided into multiple fragments. Each fragment is treated quantum mechanically, while interfragment electrostatic interactions are treated approximately using a QM/MM framework. A similar fragment-based potential, known as effective fragment potential (EFP),[7] was theoretically proposed by Gordon and co-workers. The original idea of EFP was to describe aqueous solvent effects on molecules of biological interest, where the solute was described at a chosen QM level and the solvent molecules were represented by EFPs. The EFP consists of both the long- and short-range terms that are defined by using a perturbation theory. In the EFP approach, each water molecule is represented as a fragment of fixed geometry with a set of parameters deduced from ab initio calculations. In the original implementation,[8] called EFP1, the interaction energy between water molecules consists of Coulomb, polarization, and repulsion terms. The Coulomb term is evaluated using classical multipoles up to octupoles that are centered at each atom and at bond midpoints. To account for short-range charge-penetration effects, the charge-based term in the Hamiltonian are augmented by damping functions. The fragment polarization energy is evaluated by considering the interaction of

Received: July 9, 2012
Revised: August 16, 2012
Published: August 22, 2012

   dx.doi.org/10.1021/jp306807v | J. Phys. Chem. A 2012, 116, 8965−8971

induced dipoles of each fragment with the static field due to the Coulomb multipoles as well as the induced field due to the induced dipoles of the other fragments. The induced dipoles are located at the centroids of localized molecular orbitals (LMO) at which (anisotropic) distributed polarizability tensors are placed. The remaining contribution to the ab initio−EFP interactions accounts for exchange-repulsion and charge transfer effects, which are modeled in the form of Gaussian functions. The EFP method has been successfully applied to a variety of studies on the water structures,[9,10] chemical reactions,[11,12] and photochemistry in water.[13] However, most applications are based on the geometry optimization, except for a few cases where short conformational samplings were performed.[14] It has been shown that the EFP could successfully reproduce full QM results with comparatively low computational cost note that the computational speed with EFP is orders of magnitude faster than that of typical full QM calculations.[8] Therefore, it is quite clear that the advantage of EFP as compared to classical parameters is its chemical accuracy in the calculations of energies and structures.

The applicability of the hybrid QM/EFP to long-time MD simulations of chemical reaction in water has been recently examined,[14] where it was found that the QM/EFP yields quite accurate free energy change and reaction barrier associated with the transition from the zwitterion to nonionized form of glycine in water. This demonstrates that the hybrid QM/EFP with fairly sophisticated parametrizations can indeed yield accurate energies and structures even when it is combined with MD simulation methods. Despite that there are a number of different ways to examine the accuracy of a newly developed computational method, one of the most direct and stringent tests would be to directly calculate vibrational spectra of polyatomic molecules and to compare the resulting spectra with experimental ones in a quantitative manner. Note that the vibrational frequencies and spectral lineshapes are extremely sensitive to the multidimensional potential energy surface of the solute molecules interacting with surrounding solvent molecules. Recently, the electric dipole−electric dipole and electric dipole−magnetic dipole correlation functions of a solute in solutions were directly calculated by using the QM/MM-MD trajectories, and then their Fourier-transformed spectra corresponding to the infrared (IR) absorption and vibrational circular dichroism (VCD) were compared with experimental results.[15−18] In particular, we, for the first time, showed that the combined QM/MM-MD and time-correlation function theory can provide quantitative information on the mid- and near-IR absorption and VCD bands associated with fundamental transitions as well as vibrational overtone and combination transitions of small chiral molecules in solution.[18] Furthermore, the same electric dipole correlation function approaches were extended and used to numerically calculate the two-dimensional IR spectrum of an aqueous *N*-methylacetamide solution,[19,20] where the forward−backward propagation method developed by Hasegawa and Tanimura[21] was used to calculate the nonlinear vibrational response function.

Here, as an extension of our previous studies,[14,18] we investigate the applicability of the water EFP in the simulations of the IR spectrum of solution phase. Despite that the classical MD simulation can also provide the time-correlation function of the molecular dipole moment, which is the key quantity of producing anharmonic vibrational spectra via its Fourier transformation, it is well known that the intramolecular potential functions implemented in classical MD simulations cannot accurately describe anharmonic vibrational dynamics at all due to its approximate nature of potential functions for bond stretching, internal rotation, and bending motions. In this regard, a QM treatment of a target solute molecule during MD simulations is prerequisite for successfully describing vibrational features originating from potential anharmonicity. Nevertheless, because of its increased computational complexity, such computational approach combining time-correlation function calculations and QM/MM-MD simulations has been investigated only recently.[15,16,22] Previously, the anharmonic effects on vibrational spectra have been described by including higher terms in vibrational potential energy beyond quadratic terms.[23−25] Barone and co-workers have developed a vibrational perturbative theory[25,26] to calculate the anharmonicity-corrected fundamental, overtone, and binary combination bands. Abbate and co-workers used the local mode approximation, which was initially developed by Child[27] and Henry,[28] for C−H stretching vibrations of camphor and camphorequinone and presented near-IR VCD spectra of the C−H stretching overtone transition.[29] Nevertheless, there is a notorious difficulty to explore the multidimensional anharmonic potential surface by using quantum chemical calculation methods. Thus, the complexity of the approach increases significantly as higher anharmonic terms are included in a perturbative manner. Furthermore, the ab initio calculations of even anharmonic vibrational spectra for gas phase molecules cannot provide critical information on solvatochromic vibrational frequency shifts and time scales and amplitudes of vibrational frequency fluctuations induced by solute−solvent interactions. Thus, it is believed that the present computational method combining QM/EFP-MD and time-correlation function theory will be a highly useful scheme for directly simulating anharmonic vibrational spectra in both mid- and near-IR frequency regions. As an important example, we specifically apply the QM/EFP-MD method to the calculation of the IR spectrum of methanol in water; note that the H-bonding interaction between MeOH and surrounding water molecules has strong influences on the MeOH vibrational spectra as manifested by solvatochromic frequency shifts[30] and spectral line broadenings.[31−34]

2. COMPUTATIONAL AND EXPERIMENTAL METHODS

For the calculations of gas-phase harmonic vibrational spectra in terms of normal modes, quantum mechanical calculations were first performed on a single methanol molecule with HF and MP2 methods with the 6-31G(d) basis set. Note that the double (electric and mechanical) harmonic approximations were invoked to calculate the vibrational frequencies and transition dipoles. To obtain a fully anharmonic vibrational spectrum, it is inevitable to calculate a number of anharmonic coefficients using the finite-difference method. However, even with those anharmonic parameters determined, it is still impossible to find one-to-one correspondences between calculated overtone and combination frequencies with those observed in the experimentally measured spectrum because of solute−solvent interaction-induced frequency shifts and line broadening effects. In contrast, our approach combining QM and EFP-MD simulation methods automatically takes into account the effects from anharmonic couplings between vibrational degrees of freedom because the vibrational dynamics on the QM potential function is directly simulated. Furthermore, the polarizable nature of the solute MeOH in strongly associating solvent water is naturally included in the

calculation of electric dipole moment of MeOH for each snapshot configuration.

More specifically, the anharmonic vibrational spectra of MeOH in aqueous environment were obtained by carrying out extensive QM/EFP-MD simulations. Both HF and MP2 methods with 6-31G(d) basis set were used for the QM part (MeOH) of the QM/EFP scheme. To study the effects of distant electrostatic interaction, a three layer QM/EFP/PCM[35−37] simulation was also performed for comparison (see Figure 1), where the water molecules around MeOH were

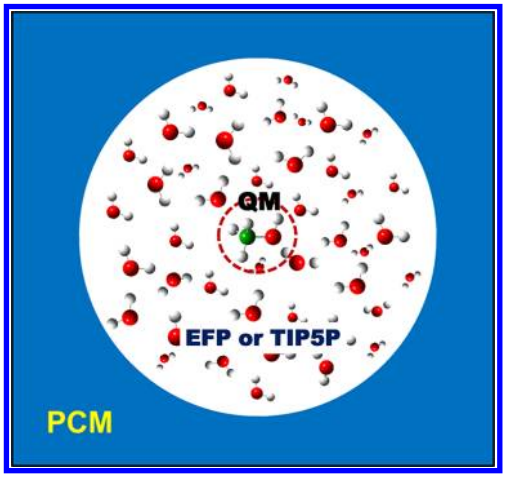

Figure 1. (a) Diagram of QM/EFP(or TIP5P)/PCM scheme for the MD simulations. The methanol and 289 waters were treated by quantum mechanics and EFP or TIP5P parameters. A spherical boundary condition with restraint force constant of 2 kcal/mol/Å^2 was used to prevent evaporation of water molecules on the surface of MeOH/water cluster during the simulations.

treated using the EFP model, and the whole MeOH/water cluster was placed inside the polarizable continuum model (PCM) solvent water. In addition to the EFP water, the classical water potential such as TIP5P[38] was also adopted for QM/TIP5P-MD simulations for the sake of comparison with the QM-based EFP model. Here, the QM-MM exchange-repulsion parameters of TIP5P used in the present work was developed by Li and implemented in GAMESS. The specific values for O, H, and lone pair are (30.1, 1.4), (−0.00042, 0.1), and (2.0, 1.4), respectively. For all of the MD simulations, a spherical system of a methanol molecule surrounded by 289 water molecules was prepared, where the average radius of the MeOH/water cluster is about 11 Å. Here, to prevent possible evaporation of water molecules on the surface of the cluster, we applied a weak harmonic restraint potential to those boundary water molecules as implemented in CHARMM.[39]

Once the dipole moment trajectories of the QM MeOH molecule are obtained, the IR absorption spectrum ($A(\omega)$) can be directly obtained by carrying out Fourier transformation of the corresponding time-autocorrelation function of solute dipole moment,[40] i.e.,

$$A(\omega) = \int_{-\infty}^{\infty} dt\ e^{i\omega t}\langle \mu(t)\cdot\mu(0)\rangle \quad (1)$$

Here, the solute dipole moment μ of each snapshot configuration was obtained by the conventional one-electron dipole integral.[41] Previously, we used an approximate method for calculating the solute dipole moment with $\mu(t) = \Sigma_{j=1}^{N} q_j(t)\ \mathbf{r}_j(t)$, where N is the number of solute atoms and $q_j(t)$ and $\mathbf{r}_j(t)$ represent the (Mulliken or Löwdin) atomic partial charge and position vector of the jth atom.[15,16,18] Note that the partial charge calculation itself is a crude approximation for describing the electron distribution of the solute so that thus calculated dipole moments obtained from snapshots extracted from QM/MM-MD trajectory were inevitably inaccurate. Nevertheless, we have shown that the anharmonic vibrational dynamics can be successfully simulated by treating the solute quantum mechanically and surrounding solvent molecules classical mechanically. Furthermore, the fluctuating charges originating from the polarizable nature of a given solute molecule are crucial in quantitatively reproducing the near IR and VCD spectra, whereas such solute charge fluctuations reflecting solute−solvent interaction dynamics are not important for the simulation of low-frequency IR bands.[18] In the present work, we calculated the one-electron dipole integral of the solute MeOH so that the resulting dipole moments are believed to be more accurate than the previous approaches to the calculation of dipole moment trajectory using atomic partial charge calculation methods. It should be emphasized that the dipole integrals were computed with the converged density of solute, which includes the effects from the solute−solvent interactions too.

For the full QM/MM-MD simulation, NVT runs of QM/EFP-MD simulations over 50 ps were initially performed at 300 K to equilibrate the system. Then, QM/EFP-MD production runs over 100 ps were continuously performed at 300 K by using the final structures of the thermally equilibrated system; note that the volume of the composite system is not a constant and that it may not be an ideal NVT ensemble even though the temperature and volume fluctuations are rather small. In the case of the QM/TIP5P-MD simulation, a 1 ns simulation was performed. The simulation time step used was 1 fs. The spectral range of the simulated vibrational spectra is essentially determined by the Nyquist critical frequency $f_c = 1/(2\Delta t)$, were Δt is the data saving time step of 1 fs. For the present computational studies, we have modified the GAMESS program to ultimately run the QM/EFP-MD simulations; note that this modified version of GAMESS will be distributed in the near future.

For the sake of direct comparisons of the present computational results with experimental data, we measured the FTIR spectrum of neat liquid MeOH, which was collected by using a JASCO FTIR spectrometer (FT/IR-4100) with 1 cm^{-1} resolution at 22 °C. The path length of the IR cell was fixed by using a 12 μm thick Teflon spacer (Harrick Scientific Products Inc.) placed in between two CaF_2 windows. Although each QM/MM-MD simulation was performed for a MeOH in water cluster, we found that the mid-IR spectrum of the neat liquid MeOH is quite similar to that extracted from the multivariate curve resolution-alternating least-squares analysis of the IR spectra of MeOH/water mixed solutions. Thus, the simulated MeOH IR spectra will be directly compared with that of neat liquid MeOH in some cases, but for detailed assignments of overtone and combination bands of our simulated spectrum, other experimental results reported previously are used.

3. RESULTS AND DISCUSSION

Recently, quite extensive experimental and ab initio calculation studies of vibrational parameters of MeOH were performed and presented by Perchard et al.[42] who used matrix-isolation IR spectroscopy to obtain the IR spectrum of MeOH trapped in

dx.doi.org/10.1021/jp306807v | J. Phys. Chem. A 2012, 116, 8965−8971

N_2 or Ne matrix. They presented detailed analysis results on the fundamental transition, overtone, and combination band frequencies. Another interesting IR spectroscopic study was reported by Huisken et al.[43] They studied vibrational spectroscopy of MeOH/water clusters, which were produced by means of adiabatic expansion of water vapor into vacuum. The C−O, C−H, or O−H stretch modes of an adsorbed MeOH molecule on the surface of liquid water cluster were selectively excited and then the vibrational predissociation of the complex was monitored by using an IR molecular beam depletion spectroscopy. Thereby, the orientation and detailed hydrogen-bonding interaction of the adsorbed MeOH molecules were elucidated. Nonetheless, the IR spectrum of MeOH dissolved in water cannot be easily obtained since the MeOH bands are spectrally overlapped with the intense bands of solvent water. Holden et al.[44] were, however, able to obtain the MeOH IR spectrum of its aqueous solution by carrying out the so-called multivariate curve resolution-alternating least-squares analysis of the IR spectra of MeOH/water mixed solutions. Thus, they reported the frequencies of the CH_3 deformation modes, combinations of OH bend and low-frequency librational mode, and CH_3 asymmetric and symmetric stretch modes (see Figure 4A in ref 44). In the present work, we shall directly compare our QM/MM MD simulated spectra of MeOH in water with these and our experimentally measured IR spectrum of neat liquid MeOH in detail.

3.1. Fundamental Transition Bands: 900−1600 cm^{-1}. In the MeOH/water solution, the long-range electrostatic and direct hydrogen bonding interactions between methanol and neighboring water molecules strongly affect the electronic structures of methanol, which makes the IR spectrum of MeOH in water significantly different from the matrix-isolation IR spectrum. Although the electrostatics is immediately operative when methanol is in water, hydrogen bond rearrangement and making-breaking dynamics accompanied with the reorientation of water molecules occur on a wide range of time scales from subpicosecond to hundreds of picoseconds. Therefore, to properly simulate such dynamic processes and their effects on vibrational spectra, MeOH/water configurations have to be sufficiently sampled, which is the main reason why one should carry out QM/MM-MD simulations for the present system.

The IR spectrum of an isolated MeOH was first calculated using HF and MP2 theories with 6-31G(d) basis set, while the solution spectra were obtained with various QM/MM-MD methods (for QM = HF and MP2 and for MM = EFP and TIP5P). The harmonic frequencies from the HF and MP2 vibrational analyses of an isolated MeOH were, as usual, scaled by 0.89 and 0.96, respectively. Thus, obtained line spectra in the domain 900−1600 cm^{-1} are shown in Figure 2. The fundamental transition bands appearing in this frequency region are related to C−O stretching (ν_8), τCH_3 rocking (ν_7, ν_{11}), COH bending (ν_6), and δCH_3 deformation (ν_5, ν_{10}, ν_4) modes. The corresponding experimental frequencies of MeOH trapped in a Ne matrix[42] were found to be 1033, 1075, 1157, 1318, 1450, 1470, and 1479 cm^{-1}, respectively, and our gas phase calculations with HF/6-31G(d) yielded 1036, 1057, 1148, 1341, 1457, 1470, and 1481 cm^{-1}, respectively. One can immediately find that the ab initio calculation results are in excellent agreement with the experimental values. It is also noted that the MP2/6-31G(d) provides quantitatively similar frequencies (see Figure 2), even though the relative dipole strengths estimated using HF slightly differ from those with MP2. Especially, the nearly similar intensities of ν_8 and ν_7 as

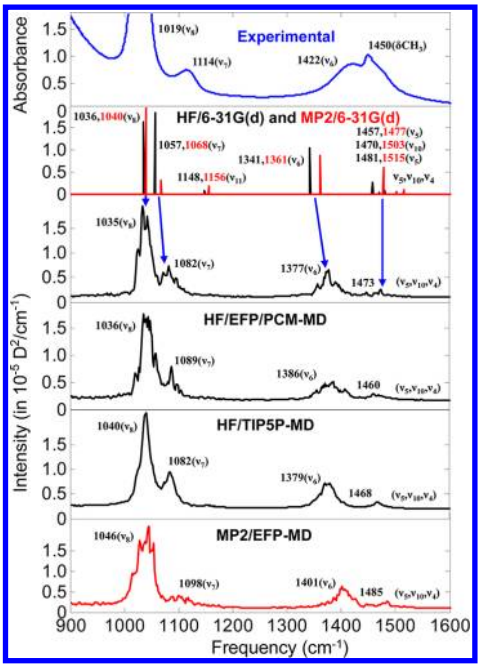

Figure 2. Experimental and predicted IR spectra in the frequency range from 900 to 1600 cm^{-1}. The gas phase spectra of methanol molecule were obtained with HF/6-31G(d) and MP2/6-31G(d). Solution spectra were obtained from the MD simulations with HF/EFP, HF/EFP/PCM, HF/TIP5P, and MP2/EFP. Here, the basis set used for the QM calculations is 6-31G(d). The experimentally measured spectrum (blue line) of neat liquid MeOH is shown for the sake of direct comparison with simulated spectra. Note that the *y*-axis of the experimental spectrum is absorbance and that of the simulated spectra is in 10^{-5} D^2/cm^{-1} (D; Debye).

obtained with HF are markedly different from those with MP2, where the ν_8 IR intensity is much stronger than the ν_7.

According to our experimental spectrum of neat liquid MeOH, there are four bands appearing at 1019, 1114, 1422, and 1450 cm^{-1}. Here, the low-frequency bands at 1019 and 1114 cm^{-1} were assigned to be the C−O stretching (ν_8) and τCH_3 rocking (ν_7) modes, respectively. The bands at 1422 and 1450 cm^{-1} were assigned to be the COH bending (ν_6) and various δCH_3 deformation modes (ν_5, ν_{10}, ν_4), respectively. One of the τCH_3 rocking modes (ν_{11}) is missing in the IR spectrum of pure liquid MeOH. Furthermore, the COH bending (ν_6) mode is strongly blue-shifted by about 104 cm^{-1} in liquid MeOH as compared to the Ne matrix-isolation experimental result.

Now, let us examine the HF/EFP-MD spectrum in Figure 2, where one can find four major peaks at 1035, 1082, 1377, and 1473 cm^{-1}, which can be easily assigned as ν_8, ν_7, ν_6, and δCH_3 deformation (ν_5, ν_{10}, ν_4). Our HF/EFP-MD clearly reproduces the disappearance of the ν_{11} band and the blue-shifting behavior of the COH bending (ν_6) mode in solution phase, which are in fact the main features found in the liquid phase MeOH spectrum. The MP2 method in the MP2/EFP-MD simulation yielded quite similar results. Not only the peak positions and intensities but also the overall lineshapes of each band in the MP2/EFP-MD spectrum are very similar to those in the HF/EFP-MD spectrum, and furthermore, such vibrational properties predicted here are in almost perfect agreement with those extracted from the experimentally measured spectrum. This suggests that, other than the peak frequencies, the HF method combined with the present MM-MD simulation method is

dx.doi.org/10.1021/jp306807v | J. Phys. Chem. A 2012, 116, 8965−8971

acceptable and equally useful in comparison to the MP2 method.

To further examine any additional distant electrostatic (dielectric) effect on the IR spectrum, we carried out HF/EFP/PCM-MD simulation and found that the resulting spectrum is quantitatively similar to the HF/EFP-MD spectrum. Therefore, the spherical water cluster with radius of 11 Å, which contains 289 water molecules, is believed to be large enough to accurately describe the solvatochromic effects of surrounding water molecules on the vibrational spectra of MeOH. In addition, we have found that the general features exhibited by the HF/TIP5P-MD spectrum, such as peak intensity distribution and band shapes and widths, are quite similar to those found in the HF/EFP-MD spectrum. Although the advantage of much more sophisticated EFP as compared to TIP5P is not apparent in the present system, it is generally expected that the EFP is capable of providing quantitatively more accurate results in other chemically reactive systems, which require a significantly more refined description of solvent−solute interaction potential.

3.2. Fundamental Transition Bands: 2700−3800 cm^{-1}. Another important region in the MeOH IR spectrum is in the domain 2700−3800 cm^{-1}. The methyl C−H (νCH_3) and methanol O−H stretch bands are shown in Figure 3. The

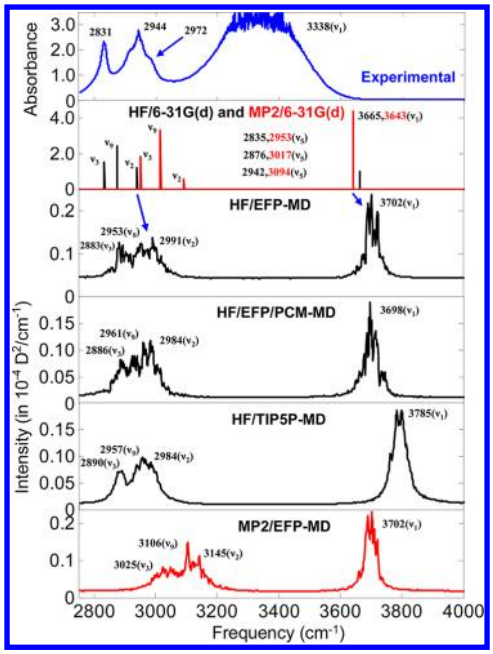

Figure 3. Experimental and predicted IR spectra in the domain 2700−3800 cm^{-1}. The asymmetric and symmetric CH_3 stretch bands and OH stretch bands appear in this region. The *y*-axis of the experimental spectrum is absorbance and that of the simulated spectra is in 10^{-4} D^2/cm^{-1}.

corresponding frequencies of MeOH trapped in Ne matrix were found to be 2841(ν_3), 2955(ν_9), 2998(ν_2), and 3690(ν_1) cm^{-1}. The gas phase frequencies obtained from the HF/6-31G(d) vibrational analysis are 2835, 2876, 2942, and 3665 cm^{-1}, respectively.

From the multicomponent analysis of a series of the IR spectra of MeOH/water mixed solutions, Holden et al.[44] showed that the CH_3 stretching band is a doublet and that the low (2837 cm^{-1}) and high (2947 cm^{-1}) frequency bands correspond to the CH_3 symmetric and asymmetric stretch modes, respectively. The corresponding peaks at 2831 and 2945 cm^{-1} are in fact observed in the experimentally measured IR spectrum of neat liquid MeOH. In particular, there appears a notable shoulder sub-band at around 2972 cm^{-1}. Our HF/EFP, HF/EFP/PCM HF/TIP5P, and MP2/EFP-MD spectra all exhibit two major peaks with the weaker low-frequency band at around 2883, 2886, 2890, and 3025 cm^{-1}, respectively. Furthermore, the shoulder sub-band at ∼2972 cm^{-1} in the experimental spectrum (the top panel of Figure 3) is also successfully reproduced by the HF/TIP5P-MD simulation, where the corresponding band appears at ∼2984 cm^{-1} in this case. Again, the HF/EFP/PCM-MD produces a nearly identical spectrum in comparison to the HF/EFP-MD spectrum, indicating that the long-range dielectric medium effects on vibrational frequencies and spectral line-broadenings are not important in this case. Here, the line shape of the OH stretching vibration is fairly similar to one another, irrespective of the QM/MM methods used, even though the peak frequency predicted is slightly dependent on the QM method, as expected. Nonetheless, the predicted fundamental transition bands of the C−H and O−H stretching vibrations are in good agreement with the experimental results. It should be emphasized that the detailed doublet features of the CH_3 stretch band cannot be easily simulated by using traditional ab initio calculations for an isolated MeOH. In this regard, the present QM/MM-MD simulation method with time correlation function approaches will thus be of critical use in understanding and interpreting experimentally measured IR spectra of even mixed solutions.

3.3. Combination and Overtone Bands: 2000−2900 cm^{-1}. As mentioned in the Introduction, one of the main advantages of the present time-correlation function approach with a QM treatment of the solute is that the vibrational anharmonicity is automatically included in the MD simulations. With the help of fundamental frequencies estimated here, it would be possible to predict that two quanta (overtone) transitions involving ν_6, ν_7, ν_8, and ν_{11} modes would appear in the frequency range from 2000 to 2900 cm^{-1}.

For this part of the discussion, the HF/TIP5P-MD spectrum obtained from a longer trajectory in comparison to others shall be mainly used; note that the signal-to-noise ratio of the HF/TIP5P-MD spectrum is much better than the other spectra, simply due to the longer simulation time (see Figure 4). In the matrix-isolation spectroscopic measurements, Perchard et al.[42] observed overtone peaks at 2051 ($2\nu_8$), 2144 ($2\nu_7$), 2305 ($2\nu_{11}$), and 2671 ($2\nu_6$) cm^{-1}. As already discussed in section 3.1 above, one of the τCH_3 rocking modes (ν_{11}) disappears in the liquid MeOH spectrum. Therefore, it is expected that its overtone may not be visible in the IR spectrum of MeOH aqueous solution sample. Now, as can be seen in the HF/TIP5P-MD spectra in Figure 4, one can easily identify the overtone bands ($2\nu_8$, $2\nu_7$, and $2\nu_6$) at 2069, 2183, and 2790 cm^{-1}.

In addition to these overtone bands, there appear four more notable bands in the domain 2000−2900 cm^{-1}. As shown in Figure 2, the fundamental transition bands of the ν_5, ν_{10}, and ν_4 modes are not clearly distinguishable, but the peak at 1468 cm^{-1} that is associated with the methyl bending vibration is visible. Thus, the peaks at 2636 and 2832 cm^{-1} in Figure 4 can be assigned to the combination modes of methyl bending with the ν_7 and ν_6 modes, respectively. Furthermore, the relatively large peaks at 2421 and 2459 cm^{-1} are likely to be the combination bands of $\nu_6 + \nu_8$ and $\nu_6 + \nu_7$, respectively. Thus,

dx.doi.org/10.1021/jp306807v | J. Phys. Chem. A 2012, 116, 8965−8971

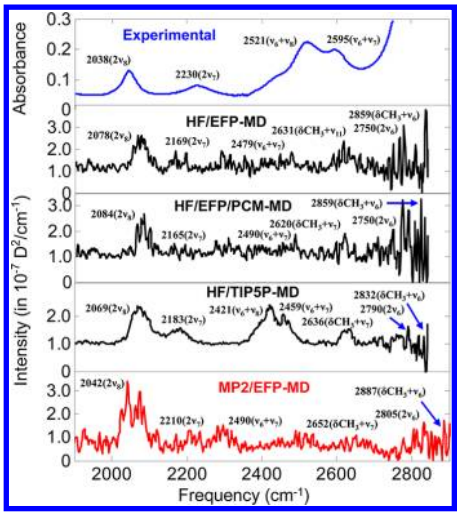

Figure 4. Experimental and predicted IR spectra in the domain 2000−2900 cm^{-1}. Note that the *y*-axis scale of the simulated spectra is in 10^{-7} D^2/cm^{-1} and that it is 2 orders of magnitude smaller than that in Figure 3.

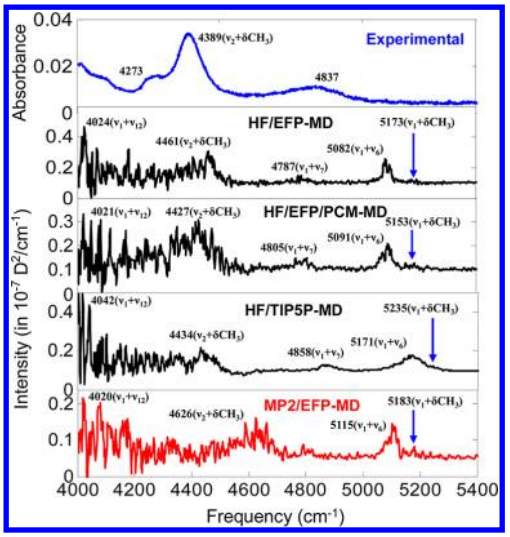

Figure 5. Experimental and predicted IR spectra in the domain 4000−5400 cm^{-1}. The *y*-axis scale of the simulated spectra is in 10^{-7} D^2/cm^{-1}, and it is about 3 orders of magnitude smaller than that in Figure 3 depicting the CH_3 symmetric and asymmetric stretch bands.

there are, in total, three overtone and four combination bands in this frequency region, and in fact, they are the major bands found in the Ne matrix-isolation IR spectroscopic measurements. Unlike the MeOH IR spectrum obtained by using the matrix-isolation spectroscopy method, the IR spectrum of our neat liquid MeOH exhibits four bands at around 2038, 2230, 2521, and 2595 cm^{-1}, which directly correspond to the four peaks at 2069 ($2\nu_8$), 2183 ($2\nu_7$), 2421 ($\nu_6 + \nu_8$), and 2459 ($\nu_6 + \nu_7$) cm^{-1} in the HF/TIP5P-MD spectrum (Figure 4). In the experimental spectrum, all the higher frequency peaks (>2600 cm^{-1}) are not discernible because they spectrally overlap with the more intense CH_3 stretch bands.

3.4. Overtone and Combination Bands: 4000−8000 cm^{-1}. In the frequency range from 4000 to 5400 cm^{-1}, other types of binary combination bands appear. For instance, it was shown that, from the Ne matrix-isolation spectroscopy, the $\nu_1 + \nu_{12}$ combination band appears at 3916 cm^{-1}. In addition, a few combination bands that are mixed modes of CH_3 stretching vibrations with lower-frequency ν_6, ν_7, and ν_8 modes were observed in the Ne matrix-isolation spectrum of MeOH. However, in our HF/TIP5P-MD simulated spectrum (Figure 5), these combination bands whose peak frequencies are smaller than 4200 cm^{-1} cannot be easily identified because they all overlap with the intense OH stretch band at around 3700−3800 cm^{-1}.

However, the combination bands of methyl stretching (νCH_3) and bending (δCH_3) modes are clearly observed in the simulated spectra in the domain 4300−4600 cm^{-1}. Experimentally, two strong peaks at 4273 and 4389 cm^{-1} were observed. They correspond to the peak at ~4434 cm^{-1} in our HF/TIP5P spectrum (Figure 5); note that these two peaks undergo solvatochromic blue-shifts and merge into a single peak in the IR spectrum of the aqueous MeOH solution. The combination bands of ν_1 with the three low frequency modes ν_6, ν_7, and ν_8 appear in the higher-frequency region. Matrix-isolation spectroscopy shows that there are relatively strong combination bands at 4757 ($\nu_1 + \nu_7$) and 5006 ($\nu_1 + \nu_6$) cm^{-1} and a weak one at 4720 ($\nu_1 + \nu_8$) cm^{-1}. Our HF/TIP5P simulated spectrum shows two strong peaks at 4858 and 5171 cm^{-1}.

The first overtones of the methyl stretching vibrations were observed in the frequency range from 5600 and 6000 cm^{-1}. We have carefully examined our simulated spectra shown in Figure 6. The peak at 5952 cm^{-1} in the HF/TIP5P-MD spectrum is

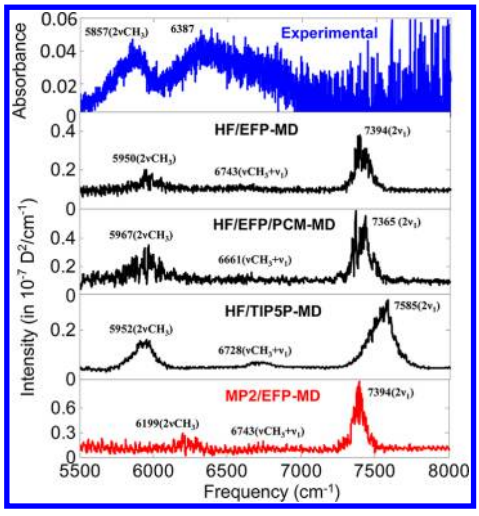

Figure 6. Experimental and predicted IR spectra in the domain 5500−8000 cm^{-1}. The *y*-axis scale of the simulated spectra is in 10^{-7} D^2/cm^{-1}, and it is about 3 orders of magnitude smaller than that in Figure 3 depicting the CH_3 symmetric and asymmetric stretch bands.

associated with the overtone bands of the CH_3 stretching vibrations. Matrix-isolation experiments also showed a combination band of CH_3 and OH stretching modes at 6616.5 cm^{-1}, which should correspond to the 6728 cm^{-1} peak in the HF/TIP5P-MD spectrum.

Finally, the OH overtone ($2\nu_1$) band at around 7400 cm^{-1} is also visible in all the QM/MM MD simulated spectra in Figure 6. Thus, not only the fundamental, overtone, and combination bands in the mid-IR frequency region but also most of the overtone and combination bands in the near IR frequency region are successfully simulated by using the present QM/MM-MD simulation method in combination with the time-

dx.doi.org/10.1021/jp306807v | J. Phys. Chem. A 2012, 116, 8965−8971

correlation function approach. Here, it should be emphasized that the *y*-axis scales of Figures 2−6 are different from one another. As expected, the overtone and combination band intensities are two to 3 orders of magnitude smaller than those of the fundamental transition bands. This observation that such weak effects originating from anharmonic couplings between vibrational degrees of freedom are quantitatively simulated by the present QM/MM-MD methods is the most important evidence for its chemical accuracy.

4. SUMMARY

The applicability of hybrid QM/MM-MD simulation methods for numerically calculating the anharmonic IR spectrum of MeOH in water has been examined in the present article. The time-correlation functions of solute dipole moments are readily obtained with the QM/EFP-MD and QM/TIP5P-MD (QM = HF and MP2) methods. It was shown that the QM/EFP and QM/TIP5P simulations provide quantitative information not only on the fundamental transition frequencies, line shapes, and relative oscillator strengths in the mid-IR region but also on the major overtone and combination bands of methanol even in the near-IR region. The simulated IR spectra were directly compared with the Ne matrix-isolation spectrum as well as that of MeOH in water. The agreement between theory and experiment was found to be quantitative. Thus, it is believed that direct calculations of anharmonic vibrational spectra can be achieved by using the hybrid QM/MM-MD simulation method. We further anticipate that the present computational protocol can be readily extended and used to simulate both one-dimensional chiroptical[18,24,45,46] and two-dimensional IR spectra[19,21,32,47,48] of biomolecules and chemically reactive systems, where the spectral intensities and lineshapes are strongly dependent on the electric and mechanical anharmonicities of molecular oscillators.

AUTHOR INFORMATION

Corresponding Author

*E-mail: cchoi@knu.ac.kr (C.H.C.); mcho@korea.ac.kr (M.C.).

Notes

The authors declare no competing financial interest.

ACKNOWLEDGMENTS

This work was supported by the National Research Foundation of Korea (NRF) grant to C.H.C. funded by the Korea government (MEST) (No. 2007-0056341 and No. 2012-0002540). M.C. is thankful for financial supports by NRF (No. 20090078897 and 20110020033) and KBSI grants (T32401).

REFERENCES

(1) Masunov, A.; Lazaridis, T. *J. Am. Chem. Soc.* **2003**, *125*, 1722.
(2) Car, R.; Parrinello, M. *Phys. Rev. Lett.* **1985**, *55*, 2471.
(3) Komeiji, Y.; Nakano, T.; Fukuzawa, K.; Ueno, Y.; Inadomi, Y.; Nemoto, T.; Uebaysai, M.; Fedorov, D. G.; Kitaura, K. *Chem. Phys. Lett.* **2003**, *372*, 342.
(4) Field, M. J.; Bash, P. A.; Karplus, M. *J. Comput. Chem.* **1990**, *11*, 700.
(5) Gao, J. L. *J. Chem. Phys.* **1998**, *109*, 2346.
(6) Xie, W.; Orozco, M.; Truhlar, D. G.; Gao, J. *J. Chem. Theory Comput.* **2009**, *5*, 459.
(7) Gordon, M. S.; Fedorov, D. G.; Pruitt, S. R.; Slipchenko, L. V. *Chem. Rev.* **2012**, *112*, 632.
(8) Day, P. N.; Jensen, J. H.; Gordon, M. S.; Webb, S. P.; Stevens, W. J.; Krauss, M.; Garmer, D.; Basch, H.; Cohen, D. *J. Chem. Phys.* **1996**, *105*, 1968.
(9) Day, P. N.; Pachter, R.; Gordon, M. S.; Merrill, G. N. *J. Chem. Phys.* **2000**, *112*, 2063.
(10) Netzloff, H. M.; Gordon, M. S. *J. Chem. Phys.* **2004**, *121*, 2711.
(11) Adamovic, I.; Gordon, M. S. *J. Phys. Chem. A* **2005**, *109*, 1629.
(12) Bandyopadhyay, P.; Gordon, M. S. *J. Chem. Phys.* **2000**, *113*, 1104.
(13) Arora, P.; Slipchenko, L. V.; Webb, S. P.; DeFusco, A.; Gordon, M. S. *J. Phys. Chem. A* **2010**, *114*, 6742.
(14) Choi, C. H.; Re, S.; Feig, M.; Sugita, Y. *Chem. Phys. Lett.* **2012**, *539*, 218.
(15) Yang, S.; Cho, M. *J. Chem. Phys.* **2005**, *123*, 134503.
(16) Yang, S.; Cho, M. *J. Chem. Phys.* **2009**, *131*, 135102.
(17) Choi, J. H.; Raleigh, D.; Cho, M. *J. Phys. Chem. Lett.* **2011**, *2*, 2158.
(18) Choi, J. H.; Cho, M. *J. Chem. Theory Comput.* **2011**, *7*, 4097.
(19) Jeon, J.; Yang, S.; Choi, J. H.; Cho, M. *Acc. Chem. Res.* **2009**, *42*, 1280.
(20) Jeon, J.; Cho, M. *New. J. Phys.* **2010**, *12*, 065001.
(21) Hasegawa, T.; Tanimura, Y. *J. Chem. Phys.* **2008**, *128*, 064511.
(22) Lindquist, B. A.; Haws, R. T.; Corcelli, S. A. *J. Phys. Chem. B* **2008**, *112*, 13991.
(23) Abbate, S.; Castiglioni, E.; Gangemi, F.; Gangemi, R.; Longhi, G. *Chirality* **2009**, *21*, E242.
(24) Abbate, S.; Gangemi, F.; Gangemi, R.; Longhi, G. *Vib. Spectrosc.* **2009**, *50*, 257.
(25) Barone, V.; Biczysko, M.; Bloino, J.; Borkowska-Panek, M.; Carnimeo, I.; Panek, P. *Int J. Quantum Chem.* **2012**, *112*, 2185.
(26) Barone, V. *J. Chem. Phys.* **2005**, *122*, 014108.
(27) Child, M. S. *Acc. Chem. Res.* **1985**, *18*, 45.
(28) Henry, B. R. *Acc. Chem. Res.* **1987**, *20*, 429.
(29) Gangemi, F.; Gangemi, R.; Longhi, G.; Abbate, S. *Vib. Spectrosc.* **2009**, *50*, 257.
(30) Cho, M. *J. Chem. Phys.* **2009**, *130*, 094505.
(31) Mukamel, S. *Principles of Nonlinear Optical Spectroscopy*; Oxford University Press: Oxford, U.K., 1995.
(32) Cho, M. *Two-Dimensional Optical Spectroscopy*; CRC Press: Boca Raton, FL, 2009.
(33) Asbury, J. B.; Steinel, T.; Fayer, M. D. *J. Lumin.* **2004**, *107*, 271.
(34) Gaffney, K. J.; Davis, P. H.; Piletic, I. R.; Levinger, N. E.; Fayer, M. D. *J. Phys. Chem. A* **2002**, *106*, 12012.
(35) Li, H. *J. Phys. Chem. A* **2011**, *115*, 11824.
(36) Si, D.; Li, H. *J. Chem. Phys.* **2011**, *135*, 144107.
(37) Li, H. *J. Chem. Phys.* **2009**, *131*, 184103.
(38) Mahoney, M. W.; Jorgensen, W. L. *J. Chem. Phys.* **2000**, *112*, 8910.
(39) Brooks, B. R.; Bruccoleri, R. E.; Olafson, B. D.; States, D. J.; Swaminathan, S.; Karplus, M. *J. Comput. Chem.* **1983**, *4*, 187.
(40) Lawrence, C. P.; Skinner, J. L. *Proc. Natl. Acad. Sci. U.S.A.* **2005**, *102*, 6720.
(41) Choi, C. H. *J. Chem. Phys.* **2004**, *120*, 3535.
(42) Perchard, J. P.; Romain, F.; Bouteiller, Y. *Chem. Phys.* **2008**, *343*, 35.
(43) Huisken, F.; Mohammad-Pooran, S.; Werhahn, O. *Chem. Phys.* **1998**, *239*, 11.
(44) Holden, C. A.; Hunnicutt, S. S.; Sanchez-Ponce, R.; Craig, J. M.; Rutan, S. C. *Appl. Spectrosc.* **2003**, *57*, 483.
(45) Rhee, H.; Choi, J. H.; Cho, M. *Acc. Chem. Res.* **2010**, *43*, 1527.
(46) Rhee, H. J.; June, Y. G.; Lee, J. S.; Lee, K. K.; Ha, J. H.; Kim, Z. H.; Jeon, S. J.; Cho, M. *Nature* **2009**, *458*, 310.
(47) Jansen, T. L. C.; Knoester, J. *Acc. Chem. Res.* **2009**, *42*, 1405.
(48) Zhuang, W.; Hayashi, T.; Mukamel, S. *Angew. Chem., Int. Ed.* **2009**, *48*, 3750.